Fuel Class VALERATES

Christine Mounaïm-Rousselle, Fabien Halter, Fabrice Foucher, Francesco Contino, Dayma Guillaume, Philippe Dagaut

Fuel Class Valerates

Christine Mounaïm-Rousselle, Fabien Halter, Fabrice Foucher, Francesco Contino, Guillaume Dayma, and Philippe Dagaut

3.1
Introduction and Fuel Properties

3.1.1
Origins of Valerate Molecules

Due to the internal structure of lignocellulose (a compound of hemicellulose, cellulose, and lignin), its conversion still remains a real challenge. Lignocellulosic biomass typically contains more than 50 wt% sugars that can be upgraded to valuable platform molecules, such as levulinic acid (LA) and γ-valerolactone (GVL), while the other ligneous parts can be used as solvents. Figure 3.1 indicates one possible roadmap proposed by Azadi *et al.* [1] for different transformations of these three components and their potential uses.

Geboers *et al.* [2] described the opportunities, advances, and pitfalls in the conversion of cellulose and stressed that while it is generally agreed that cellulose will be the basis for many future technologies, it is important to note that the only way to achieve this is not to produce "chemicals for the chemical industry" but biofuels and fine chemicals.

Valeric acid (VA) esters, called *valerates* or *pentanoates*, are derivatives of GVL. As pointed out by Chalid [3], several applications of GVL already exist in the food and perfume industries and drug delivery systems (especially due to its herbal odor) [4, 5], but GVL can also be used as a green solvent. Potential applications such as an oxygenate in transportation fuels, a comonomer for the preparation of polymers [6], or a precursor for long-chain alkanes to be used as hydrocarbon fuels [7] are quite new and have been studied for less than 10 years. Further reinforcing the potential of GVL as a biofuel platform chemical, Bond *et al.* [8] reported its conversion to liquid C_8 alkenes for fuel applications.

Valerates themselves, especially ethyl and methyl pentanoate, are commonly used not only in fragrances, beauty care, soap, and laundry detergents at levels of 0.1 – 1% but also in food due to their fruit flavor. In a very pure form (greater than

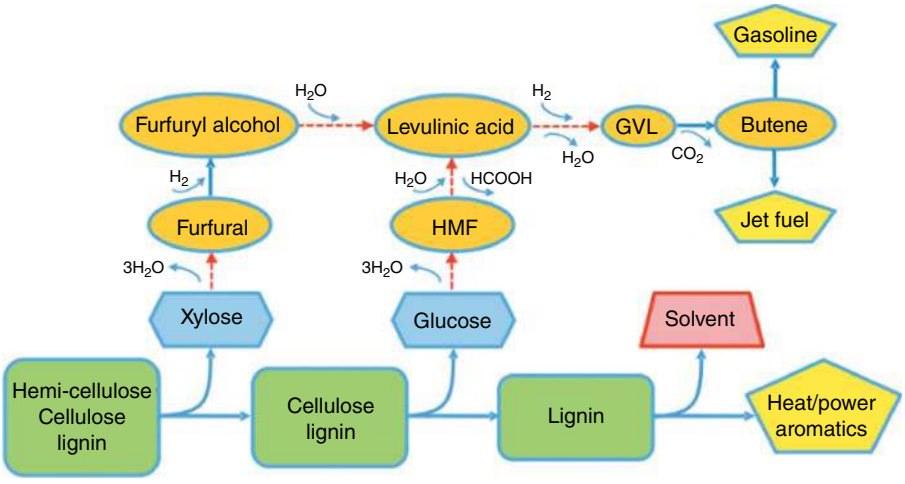

Figure 3.1 Roadmap for the conversion of lignocellulosic biomass (rectangles) to chemicals (ovals) and fuels (pentagons), via the intermediate formation of C5 and C6 sugars (hexagons), suggested by Azadi *et al.* (Reproduced with permission from Azadi *et al.* [1] of Royal Society of Chemistry.)

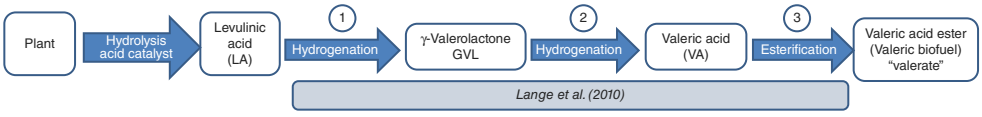

Figure 3.2 Four-step process from lignocellulose to valerate proposed by Lange *et al.* [9].

99.5%), methyl pentanoate is used as a plasticizer in the manufacture of plastics and also as an insecticide.

3.1.2
Valerates as Fuel for Internal Combustion Engines

Since 2004, researchers at Shell have developed this "new" generation of biofuels, valeric biofuels. Lange *et al.* described in 2010 the process to produce these levulinic acid derivatives from lignocellulose. These fuels are more suitable than GVL itself because they can provide biofuels that have similar properties and that can be either blended with gasoline or diesel or used as fuels themselves. The process developed by Lange *et al.* at Shell is schematized in Figure 3.2. It involves the following four steps: the classical production of levulinic acid by the acid hydrolysis of lignocellulosic materials, the hydrogenation of LA ($C_5H_8O_3$) to obtain GVL ($C_5H_8O_2$) and of GVL to obtain valeric acid ($C_5H_{10}O_2$), and finally the esterification of VA to produce a valerate.

After the final step, that is, esterification, the biofuel may be in the form of biogasoline or biodiesel, depending on the reactants used, and can be mixed with other currently available fuels. The choice of alcohol (ethanol, methanol, propanol, butanol, or pentanol) provides different valerates (respectively, ethyl valerate EV,

methyl valerate MV, propyl valerate PRV, butyl valerate BV, and pentyl valerate PV), inducing different properties.

Lange *et al.* [9] first identified some properties of the different valerate molecules such as the blending research octane number (BRON) and the boiling point. They also identified properties of some other biofuels such as alcohols and fatty acid methyl esters (FAME) or other levulinic acids (MTHF, methyl tetrahydrofuran, or EL, ethyl levulinate). The lighter esters are more suitable for spark-ignition (SI) engines and the heavier esters for diesel engines.

The properties of the five VA esters are summarized in Table 3.1.

To improve our knowledge of these fuels' properties, new experiments have been performed in a homogeneous combustion engine to determine some "optimum" regions where each fuel can autoignite and where 50% of fuel has burned between 1 and 5 crank angle degrees (CAD), as performed by Masurier *et al.* [10] for other specificities. Experiments were performed, for each fuel, at different intake temperatures and by varying the intake pressure. For each experiment, the CA50 was determined and only the data points with a CA50 ranging from 1 to 5 CAD were conserved to draw the map. The modified PSA engine used for the experiments is fully described in Refs. [11] and [10]. For the experiments, six primary reference fuels (PRFs) (mixtures of *iso*-octane and *n*-heptane) were used: PRF0, 20, 40, 60, 80, 100, with, respectively, 0, 20, 40, 60, 80, 100 vol% of *iso*-octane.

The results are plotted in Figure 3.3, where the upper limit of each fuel is an *iso*-CAD50 for 1 CAD and the lower limit is for 5 CAD. As expected, the fuels are classified according to the BRON: the highest BRON (PR100) requires high intake pressure and temperature to ignite. So for this presentation of fuel properties regarding homogeneous ignition, valerates can be divided into two categories: fuels for SI engines (EV, MV) and fuels for compression-ignition (CI) engines

Table 3.1 Properties of valerates as fuels.

Fuel	Structure	MW (g/mol)	O_2 (wt%)	LHV (MJ/kg)	AFR_{st} (kg/kg)	T_b (K)	BRON Lange *et al.* [9]	DCN ASTM D7668	ΔH_{vap} (kJ/kg at 298 K)	Density (kg/l)
Methyl valerate	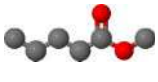	116	27.5	28.8	9.52	410	115	n.a.	371	0.875
Ethyl valerate	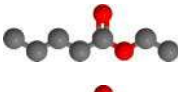	130	24.6	30.3	10.09	415	100	17.1	361	0.874
Propyl valerate		144	22.2	31.5	10.55	440	90	n.a.	277	0.870
Butyl valerate	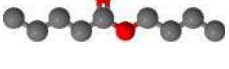	158	20.2	32.6	10.92	460	n.a.	24.5	335	0.868
Pentyl valerate	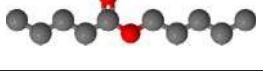	172	18.6	33.5	11.24	479	10	30.3	257	0.874

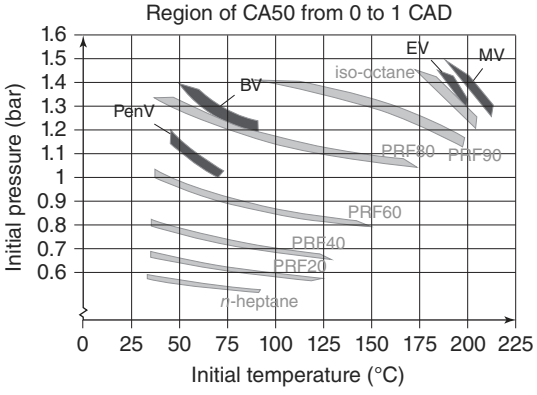

Figure 3.3 Optimum ignition conditions for valerates as fuel compared with PRF.

(BV and PenV). These results are in good agreement with the properties presented by Lange *et al.* [9].

3.1.3
Kinetic Properties of Valerate Fuels

From a chemical kinetic point of view, alkyl esters have been shown to behave similarly to alkanes [12–14], with potentially a cool flame, a negative temperature coefficient (NTC), and high-temperature reactivity, depending on the length of the carbon chain. Methyl esters (from C_2 up to C_{19}) have been extensively studied over the past decade, and the only difference with alkanes as far as reactivity is concerned lies in the influence of the carbonyl group on the neighboring carbon (carbon #2). Indeed, El-Nahas *et al.* [15] calculated the bond dissociation energies in the case of methyl butanoate and ethyl propanoate and demonstrated the relative weakness of the C–H and C–C bonds neighboring the carbonyl group. In addition, it is well accepted that the shorter the carbon chain is, the greater the impact this weakness has on the reactivity. In the particular case of valerates, the carbon chain on the acid side involves five carbon atoms. Thus, the peculiarity of carbon #2 cannot be neglected and alkyl propenoates are expected to be important intermediates. In addition, from ethyl valerate to pentyl valerate, a molecular reaction yielding valeric acid (pentanoic acid) and an olefin (from ethylene to 1-pentene) was also shown to be of primary importance at high temperature (above 800 K) [12]. Moreover, Hayes and Burgess [16] investigated theoretically the early CO_2 production observed during methyl ester combustion. These three elements make the oxidation of valerates important when studying the use of these compounds as fuels.

In the literature, ignition delays were only measured in a rapid compression machine for methyl valerate/air mixtures by Hadj-Ali *et al.* [14]. In their study, the authors compared the ignition characteristics of different methyl esters and *n*-alkanes over the low and intermediate temperature ranges (650–850 K) and for

pressures between 4 and 20 bar. Under these conditions, methyl valerate exhibits a two-stage autoignition, with a clearly identified cool flame event. No kinetic mechanism was proposed for methyl valerate autoignition in the study. Moreover, no ignition delays measured in shock tubes are reported in the literature for alkyl valerates and detailed kinetic modeling suffers from this lack of experimental data.

As far as spark ignition is concerned, laminar burning velocities, $S_L°$, were measured for ethyl and methyl valerate/air mixtures by Contino *et al.* [17] in a spherical combustion chamber at $T_u = 423$ K (the fresh gas temperature), at two initial pressures ($p = 1$ and 3 bar), and for equivalence ratios (φ) ranging from 0.7 to 1.4. As can be seen from Figure 3.4a, $S_L°$ reaches a maximum around $\varphi = 1.1$ and the laminar burning velocities for EV are slightly higher than those of MV and *iso*-octane. For ethyl valerate at stoichiometric ratio, a negative dependence on pressure was observed (Figure 3.4b). A detailed kinetic mechanism able to reproduce these experimental data was proposed, and these laminar burning velocities were shown to depend mainly on reactions belonging to the C_0–C_1 submechanism and involving H atoms.

The flame structures of methyl and ethyl valerate were also investigated by Shmakov *et al.* [18] and Knyazkov *et al.* [19], respectively. In both of these studies, the authors probed the flames at different heights above the burner and reported mole fractions of several species (fuel, intermediates, etc.) as a function of this height. Shmakov *et al.* [18] studied stoichiometric and rich methyl valerate/O_2/Ar flames at low and atmospheric pressures using molecular beam mass spectrometry with tunable synchrotron vacuum ultraviolet photoionization for low-pressure flames and soft electron impact ionization for atmospheric

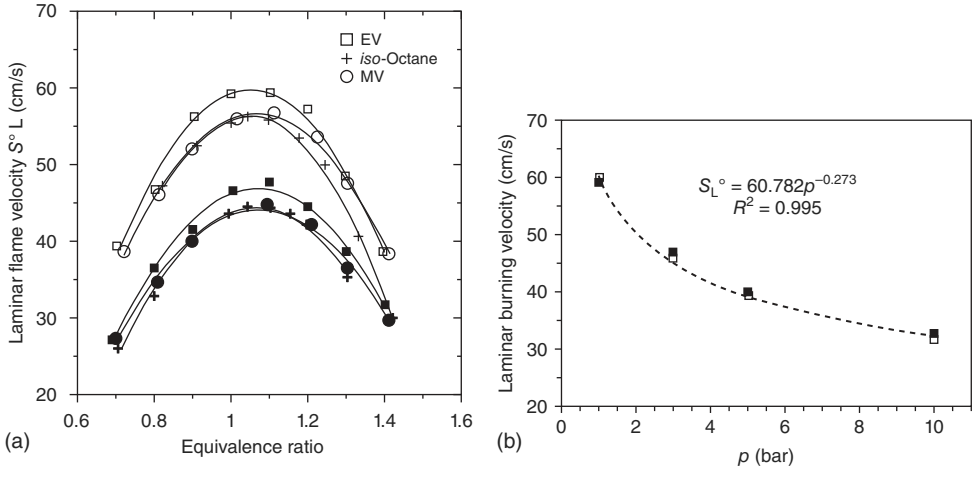

Figure 3.4 Experimental values of laminar burning velocities of ethyl and methyl pentanoate/air mixtures at $T = 423$ K (a) as a function of the equivalence ratio at 1 bar (filled symbols) and 3 bar (open symbols). Comparison with *iso*-octane. (b) Laminar burning velocity for EV as a function of the pressure at $\varphi = 1$ (filled symbols: data; open symbols and dashed line: computations).

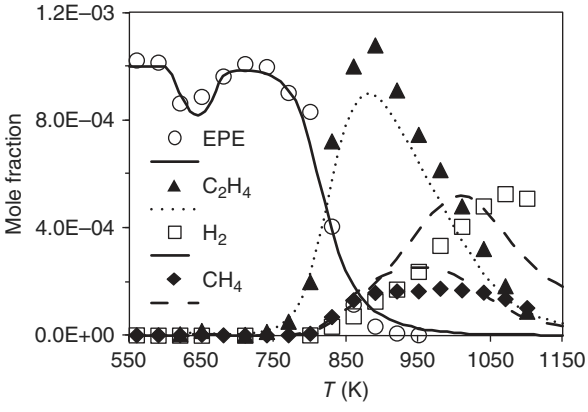

Figure 3.5 Experimental (symbols) and computed (lines) mole fraction profiles obtained from the oxidation of ethyl pentanoate in a JSR at $\varphi = 1$, $p = 10$ atm, $\tau = 0.7$ s (EPE, ethyl pentanoate).

flames. A kinetic mechanism was validated using these experimental results. Knyazkov *et al.* [19] focused on low-pressure ethyl valerate/O_2/Ar flames using molecular beam mass spectrometry with vacuum ultraviolet photoionization and found that the calculations performed using the kinetic mechanism developed by Dayma *et al.* [12] were in good agreement with their experimental data.

Mbuyi Katshiatshia *et al.* [20] also provided new data on a rich premixed flat flame of ethyl valerate/O_2/Ar at low pressure in order to validate and improve the mechanism proposed by Dayma *et al.* [21].

Lastly, ethyl valerate oxidation was also studied in a jet-stirred reactor (JSR) at a high pressure (10 atm), for three different equivalence ratios (0.6, 1, and 2), and over a wide range of temperatures (560–1160 K) by Dayma *et al.* [12]. Mole fraction profiles were reported as a function of the temperature for several stable compounds, among which are pentanoic acid and ethyl propenoate. A cool flame and an NTC were observed and the detailed kinetic mechanism developed was well able to reproduce the experimental data, as shown in Figure 3.5.

Preliminary results on extensive road tests [9] for gasoline mixed with 15% by volume of ethyl valerate showed no negative impacts on engine running, fuel tank, and fuel lines after a total distance of 250 000 km.

The following sections first present the performance of methyl and ethyl valerate in a spark-ignition engine and then the performance of butyl and pentyl valerate in a compression-ignition engine.

3.2
Performance in Spark-Ignition Engines

Lange *et al.* [9] mention tests of engines operated with valeric biofuels. In their study, 10 current types of vehicle, representative of the current market

technologies, were fueled exclusively with a mixture of normal gasoline mixed with 15% by volume of ethyl valerate and were sent out on the road to cover 500 km/day. Compared to methyl valerate, ethyl valerate benefits of a higher volumetric energy content. To further investigate the potential of valeric biofuels, we first tested pure and blends fuels in two different single-cylinder SI engines but with different and complementary evaluation of their performances as fuels.

3.2.1
Global Performance of SI Engine Fueled with Valerate Blend and Pure Valerates

To improve the results obtained by Lange *et al.*, both blended fuels and pure fuels of MEV and EV were tested, and to compare the performance, gasoline was not used but a mixture of *iso*-octane/*n*-heptane, a PRF (PRF95), with 95% of *iso*-octane as SP95.

Experimental Setup

The experiments were carried out in a four-cylinder SI engine (PSA EP6) converted into single-cylinder operation. This engine has a four-valve pent-roof chamber with a displacement volume of 399.5 cm^3/cylinder and a compression ratio of 10.5. The bore, stroke, and connecting rod lengths are 77, 85.8, and 138.5 mm respectively. The engine, driven by an electric motor, was kept at a fixed engine speed: 1500 and 2500 rpm. The intake air, supplied by an air compressor, was dehumidified to a dew point of 4 °C and electrically heated to keep the temperature in the range 45–50 °C. This air flow was metered and controlled by a Brooks flow meter to obtain an intake pressure ranging from 0.4 to 1 bar. The fuel flow from a pressurized tank was metered and controlled by a 0–8 kg/h Bronkhorst Coriolis flow sensor with a maximum combined standard uncertainty of ±1% for the minimum flow rate considered in the present work. The fuel was fully premixed with the intake air by supplying a fuel/air mixture from a heated fuel-vaporization chamber upstream of the intake plenum (see Figure 3.6). The mixture was ignited by a conventional spark plug with an electrode space of 1 mm, and the spark timing was optimized to maintain a crank angle of maximum pressure around 12 ± 0.5 Degree after top dead center (TDC) for the various loads (from 2 to 9 bar indicated mean effective pressure (IMEP)) and speeds.

Cylinder pressure was recorded with a water-cooled AVL quartz pressure transducer connected to a charge amplifier. The acquisition was performed every 0.1 CAD through an optical encoder mounted on the main shaft. A timer card ensured synchronization of the various trigger signals and data acquisition systems. The average values presented result from 100 consecutive cycles and were analyzed following the method described in Refs. [22, 23].

The exhaust emissions of nitric oxides (NO_x), unburned hydrocarbon (UHC), methane (CH_4), carbon monoxide (CO), carbon dioxide (CO_2), and oxygen (O_2) were measured by an Environnement S.A. emission analyzer with an accuracy of

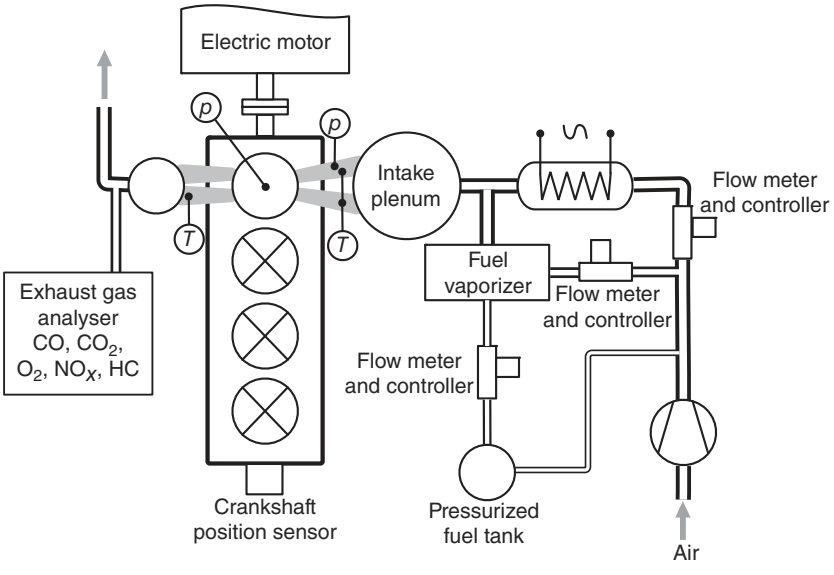

Figure 3.6 Single-cylinder SI engine bench.

1% of full scale (HC: 10 000 ppm, CH_4: 1000 ppm, CO: 5000 ppm and 10%, CO_2: 20%, and O_2: 25%).

Main Results

The thermal efficiencies obtained from the experimental results for all mixtures and speeds are shown in Figure 3.7. As expected, thermal efficiency increases with load as the inlet pressure increases and the pumping losses decrease. There is no significant difference between the reference fuel PRF95 and the mixture of valeric esters with PRF95, at 1500 rpm (empty symbols) and 2500 rpm (filled symbols). Only the error bars for PRF95 are presented but are similar to all other fuels at the same load. The CO_2 emissions are linked to the efficiency evolution. However, the mass of carbon per unit energy in the fuel should be considered to explain the higher CO_2 emission for the valeric esters compared to PRF95 (67.7 g_c/kW h_{fuel}): 77.6 and 76.8 g_c/kW h_{fuel} for MV and EV, respectively.

For the following results, only the experiments at 1500 rpm and for pure PRF95, MV, and EV are presented for the sake of clarity, as the effect of 20% of valerate blend is not distinguishable.

The exhaust emissions of nitric oxides (NO_x) and UHCs are presented in Figure 3.8. The differences in NO_x concentration are within the error bars, but a slight decrease can be observed when using valeric esters. On the other hand, the HC emissions are slightly higher at high loads and lower at low loads. The small variability observed throughout the different loads might explain this tendency.

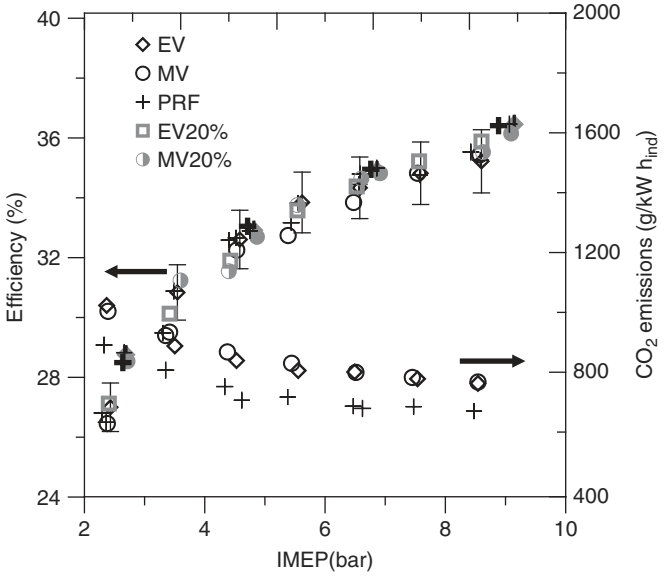

Figure 3.7 Efficiency and CO_2 emissions as a function of IMEP for EV, MV, PRF as fuel, and 20% EV and MV blends. The open symbol is for 1500 rpm and the filled one for 2500 rpm. (Reproduced with permission from Contino [17] of SAE International.)

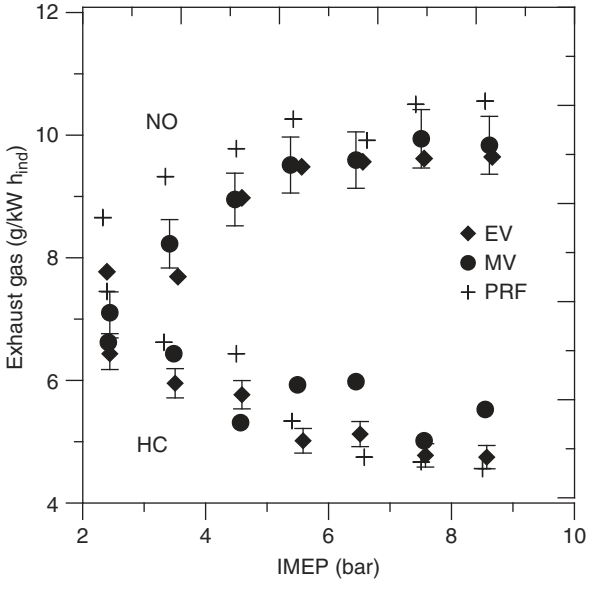

Figure 3.8 NO and UHC emissions for pure fuels as a function of IMEP.

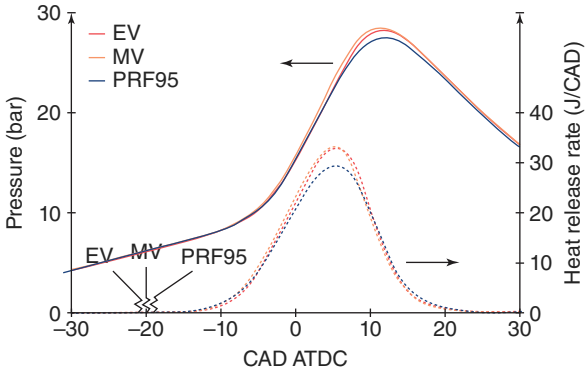

Figure 3.9 Example of cylinder pressure and HRR evolutions for MV, EV, and PRF95 (intake pressure = 0.6 bar, IMEP = 4.5 bar).

The CO emissions for the various fuels are similar and no specific trend was observed [24].

An example of pressure traces and corresponding heat release rates (HRRs)at mid-load (IMEP = 4.5 bar) are presented in Figure 3.9. The HRRs of the valeric esters are slightly above that of PRF95 due to the slightly higher amount of energy injected in the combustion chamber under stoichiometric conditions. The spark timing (indicated in the figure) was adjusted to keep the crank angle of maximum pressure at 12 ± 0.5 CAD due to the difference in laminar burning speed as shown in Figure 3.4a.

Finally, in addition to the BRON (Table 3.1), we performed ignition delay simulations of methyl and ethyl valerate compared to PRF95. The mechanism of Curran *et al.* [25] was used for PRF95, the mechanism developed by Dayma *et al.* [21] was used for ethyl valerate, and a currently developed mechanism was used for methyl valerate. The simulations were performed with the TDAC method [17, 22, 26] at 40 bar and $\Phi = 1$ for a range of temperatures between 800 and 1200 K. The ignition delay was defined as the maximum pressure rise rate in an adiabatic vessel. As expected from the BRON values, MV and EV are significantly more resistant to autoignition compared to PRF95 (see Figure 3.10). An inversion is observed between EV and MV around 990 K, which needs to be investigated with future experimental results.

A second series of experiments was performed in another single-cylinder port-fuel-injection SI engine with pure fuels (MV, EV), compared to *iso*-octane. The main interest of this study was to measure nonregulated pollutant emissions.

3.2.2
Specific Consumptions and Nonregulated Pollutant Emissions for Pure Valerates

The setup was fully described in Ref. [27]. The global characteristics are summarized here. The four-valve pent-roof combustion chamber of the single cylinder

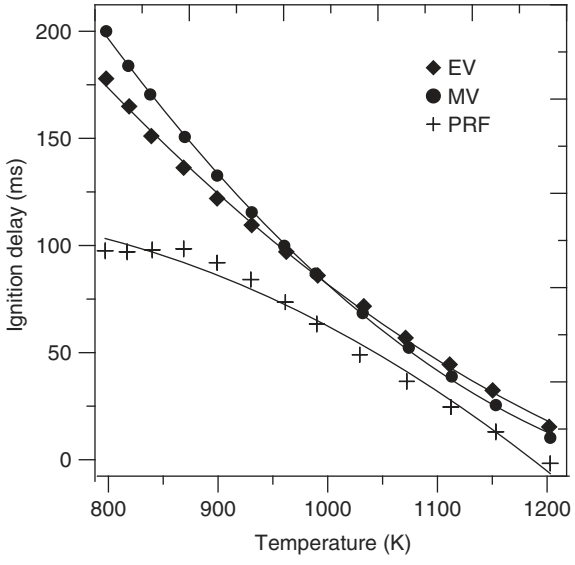

Figure 3.10 Estimated ignition delay for MV and EV at different temperatures.

is characterized by a displacement volume of 499 cm^3 and a compression ratio of 9.5. The bore, stroke, and connecting rode lengths were, respectively, 88, 82, and 137 mm. The oil and coolant temperatures were fixed at 80 °C and the intake temperature at 23 °C. A common spark plug, with an electrode space of 1 mm, equipped the engine. The engine was fed by pressurized air through a volume flow meter with an accuracy of ±0.7% on the instantaneous flow. Before the intake pipe, all the gases passed through a plenum volume, to avoid pressure oscillations inside the intake port. The liquid fuel was measured by using a 0–8 kg/h Brooks Quantim (QMBM) Coriolis mass flow meter with a maximum combined standard uncertainty of ±1% for the minimum flow rate considered in the present work. An optical encoder mounted on the crankshaft, giving a 0.1 CAD as resolution, was used with a water-cooled AVL quartz pressure transducer connected to a charge amplifier to record in-cylinder pressure. An Environnement S.A. 5 gas emission tester was used to measure the regulated emissions, with an accuracy <2% of the measured value and 1% of full scale. For the nonregulated emissions, an Environnement S.A. Fourier transform infrared spectroscopy (FTIR) was used to measure in particular CH_4 (methane), C_2H_2 (ethylene), C_6H_6 (benzene), HCOH (formaldehyde), and CH_3HCO (acetaldehyde), with an accuracy <2% of full scale (Table 3.2).

Only two operating points were selected for this study to represent middle and low engine operating conditions, the three different fuels are studied, and the spark timing is adjusted to maximize IMEP.

Use of valeric biofuels induced a small diminution of the timing advance due to higher reactivity for valeric biofuels, confirmed by laminar burning velocity measurements (Figure 3.4a).

Table 3.2 Operating conditions for unregulated pollutant emission study.

Case	Regime (rpm)	Intake pressure (bar)	Optimized IMEP (bar)	Equivalence ratio
Case 1	2000	0.64	5	1
Case 2	1700	0.5	3	0.81

The specific consumptions (g/kW h) are plotted in Figure 3.11 versus the low heating values (LHV). As the IMEP is kept constant for each condition, the specific consumption is directly sensitive to the fuel consumption in mass. The specific consumption is observed to decrease linearly with the LHV, with a notable low value in the case of *iso*-octane.

By considering the specific consumption in volume and not in mass, the biofuels partly catch up. Indeed, the density of the biofuels is higher than that of *iso*-octane (0.692 kg/l for *iso*-octane, 0.875 kg/l for MV, and 0.875 kg/l for EV).

The molecular structure of valeric biofuels, which contain oxygen atoms, slightly counterbalances the higher consumption. UHC emissions are mainly generated by incomplete combustion. UHC emissions divided by the specific consumption are reported in Figure 3.12.

iso-Octane exhibits the largest UHC emissions, twice higher than the other two, for both cases. Methyl and ethyl valerates have almost the same level of emissions. UHC emissions are dependent on the (H/C) ratio, which is 2 for the valeric biofuels

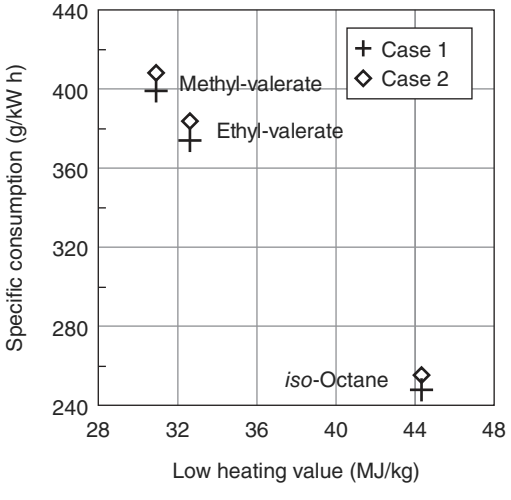

Figure 3.11 Specific consumption as a function of the low heating value for the three different fuels for both conditions.

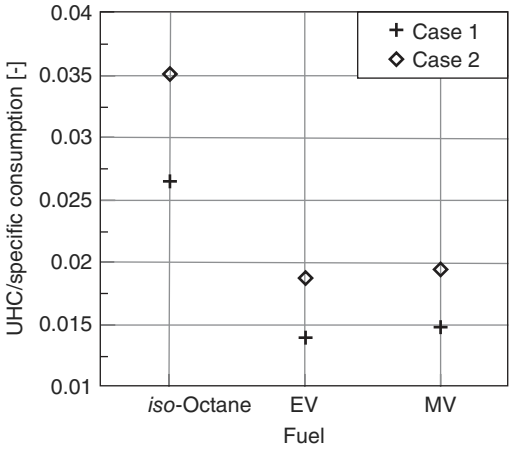

Figure 3.12 Unburned hydrocarbons (UHC) emissions for all fuels.

and 2.25 for *iso*-octane. This could slightly reduce the differences. No noticeable differences were observed concerning NO_x emissions, mainly due to burnt gases' temperature and the chemical residence time. Concerning CO, the presence of oxygen atoms in the valerates does not induce large modifications in CO emissions as it was previously demonstrated with alcoholic fuels [27].

As a precursor of several species such as formaldehyde, methane, and acetylene, the impact of ethylene involves its determination (Figure 3.13).

A large increase in ethylene emissions is observed when valeric fuels are used, and almost no ethylene is emitted when running the engine with *iso*-octane. With methyl valerate, the value reaches around 1.4 and 2.0 kg/kW h with ethyl valerate.

Methane has an impact both on global warming and on air pollution. A large decrease in methane emissions is observed when using valeric biofuels (Figure 3.13b). This diminution is more pronounced with ethyl valerate. These trends are directly opposed to those of ethylene. The main precursors of methane formation are CH_3, C_2H_4, and C_8H_{18}. As a result, it is evident that the production of methane is enhanced by the use of *iso*-octane as fuel. Then, using fuels containing oxygen atoms favors the transformation of CH_3 in CH_3O and not in methane. Finally, the path via C_2H_4 seems to be inhibited when burning methyl valerate and especially ethyl valerate.

Benzene (C_6H_6) is known to be carcinogenic and a soot precursor. A strong reduction in benzene emissions was observed when fueling the engine with alkyl valerates (Figure 3.13c) and equal to zero with ethyl valerate.

Formaldehyde has already been regulated in California due to its carcinogenic specificity (low emission vehicle (LEV II) standards, http://transportpolicy.net). Methyl valerate exhibits larger values of formaldehyde emissions, whereas ethyl valerate presents values only slightly higher than that of *iso*-octane. As said previously, fuels containing oxygen atoms favor the transformation of CH_3 in CH_3O.

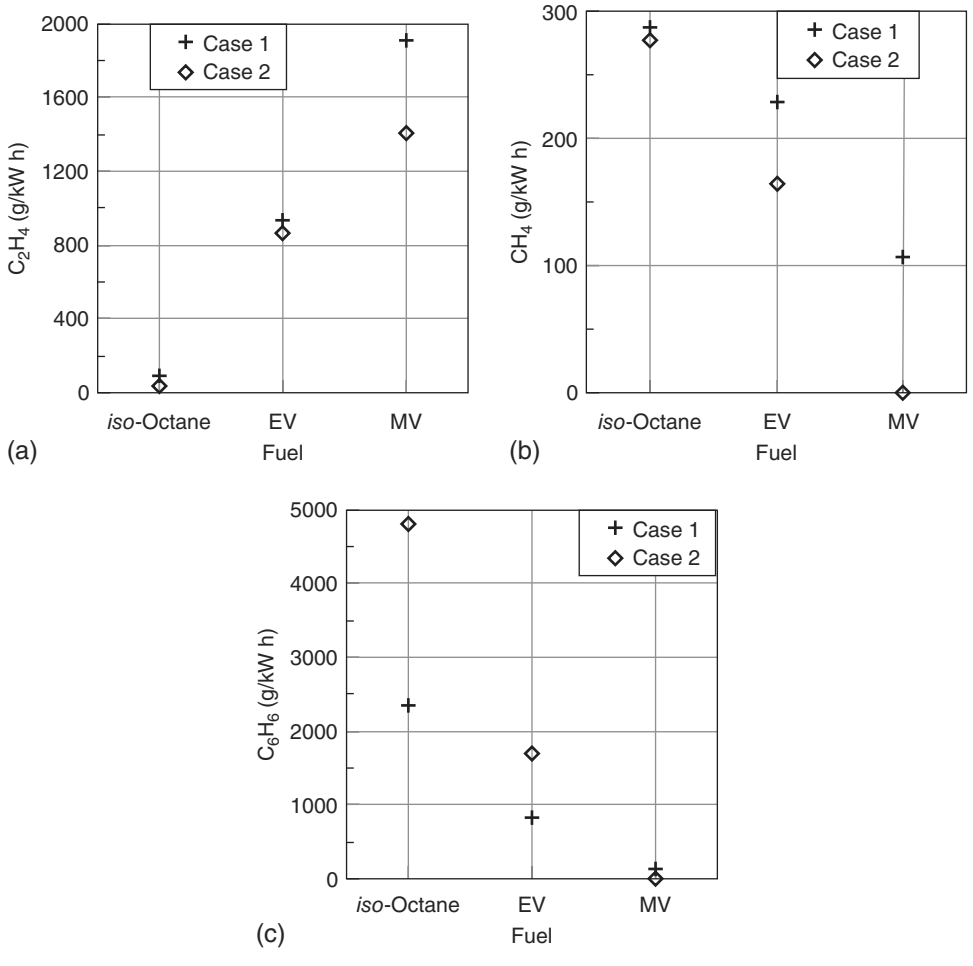

Figure 3.13 Ethylene, methane, and benzene emissions for all fuels and under both engine conditions.

These results have demonstrated the ability of both these fuels to be directly used in a spark-ignition engine, but the limitation is due to their higher consumption.

The new results in single-cylinder engines confirm the previous results of Lange *et al.* [9]: no significant differences were observed for emissions and performances when running the engine with pure esters compared with PRF95. As valerates have a higher laminar burning speed, spark timing needs to be adjusted to keep the crank angle of maximum pressure constant and to reach the optimal working point. Moreover, according to the Research Octane Number and numerical simulations of ignition delay, the esters are more resistant to autoignition. Accordingly, methyl and ethyl valerates are very interesting fuel additives or alternatives to gasoline.

Similar experiments were performed for a CI engine with blends of 20 vol% BV and PenV in diesel fuel, compared with pure diesel fuel [17, 22]. A single-cylinder CI engine, based on a four-cylinder PSA DW10 engine (see Figure 3.14) was used (a displacement volume of 499 cm^3/cylinder, the bore, stroke, and connecting rod lengths are 85, 88, and 145 mm, respectively, and the compression ratio is 16.7.

Air from a compressor is filtered, dehumidified, and preheated before the intake plenum. The fuel is injected in the combustion chamber using a seven-hole Bosch CRI 3.1 injector. A valve located after the exhaust plenum regulates the back pressure at the same value as the inlet pressure. Temperature (type K thermocouple) and absolute pressure (Kistler 4075A piezoresistive absolute pressure sensor) are measured in the intake and exhaust ports. The cylinder pressure is measured by a Kistler 6043A piezoelectric transducer at 0.1 CAD increments. The composition of the exhaust gas is measured with the Environnement S.A. emission analyzer. The smoke content is measured with an AVL 415 smoke meter.

For all experiments, the engine speed, driven by an electric motor, was set at 1200 rpm. The inlet pressure and temperature were kept constant at 1.1 bar and 40 °C, respectively. The engine was preheated by lube oil and cooling water at 88 and 94 °C, respectively, during the whole experiment. The fuel injection was split in two parts: approximately one-third of the fuel was injected as a pilot injection at 8 CAD before TDC and the remaining at 4 CAD after TDC. The injection pressure was set to 1000 bar, and the injection duration was adapted to cover a range of IMEP from 2 to 7.

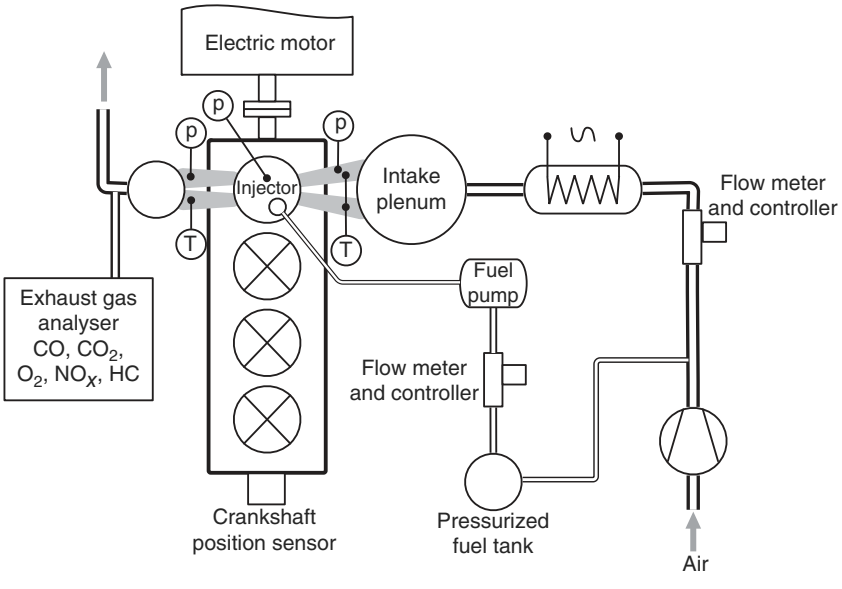

Figure 3.14 Compression-ignition single-cylinder bench.

To compare the different fuels, the injection timing was not optimized for each load or fuel blend but was kept constant so that the fuels could be compared under the same thermodynamic conditions. More details about the experimental setup and uncertainty analysis are provided in Ref. [24]. For all results, only average values are presented and error bars are plotted for the BV blend only.

As can be seen in Figure 3.15, where only average values are presented, the indicated efficiency increases with the IMEP up to around 4.5 bar and then decreases.

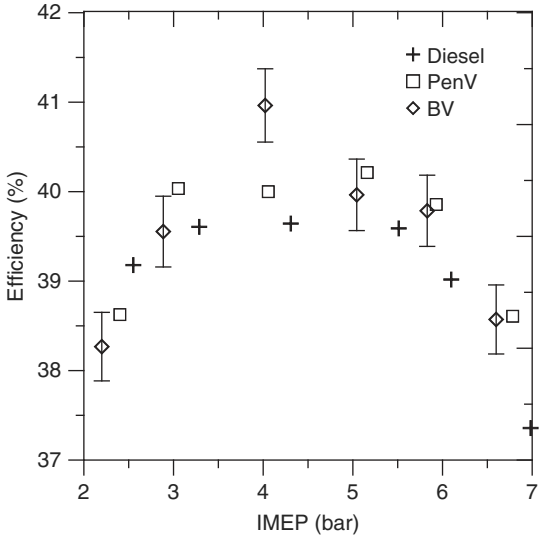

Figure 3.15 Indicated efficiency as a function of IMEP for diesel and blends with 20% of BV and PenV.

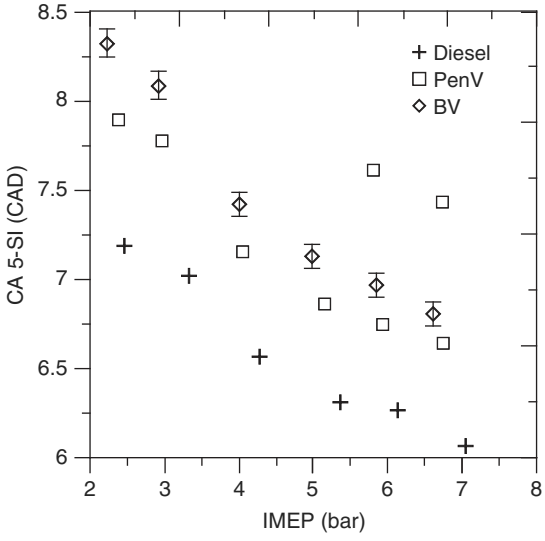

Figure 3.16 Ignition delay determined by CA5-SI_1 for BV and PenV in comparison with diesel.

While there is a slight increase in the carbon content when adding 20 vol% of valeric esters, the CO_2 emissions were found to be linked to the efficiency evolution (carbon content was 72.8 and 73.0 g/kW h_{fuel} for the blend with butyl and pentyl valerate, respectively, compared to 72.7 g/kW h_{fuel} for diesel fuel).

As shown in Table 3.1, the cetane number of valerates is less than that of diesel fuel. To determine the ignition delay of the valerates, the difference between the crank angle corresponding to when 5% of fresh gases (CA5) have been burned and the crank angle corresponding to the injection timing (SI) was plotted (Figure 3.16). The ignition delay of the blend with pentyl valerate is slightly shorter than that with butyl valerate, but overall at 1200 rpm, there is a difference of 0.8 CAD for CA5-SI_1 between the diesel fuel and the blends.

In Figure 3.17a, the CO emissions significantly decrease until 5 bar and increase after 6 bar, indicating a lower combustion efficiency. The emissions for blends are higher than those for pure diesel fuel. The same trends can be observed for

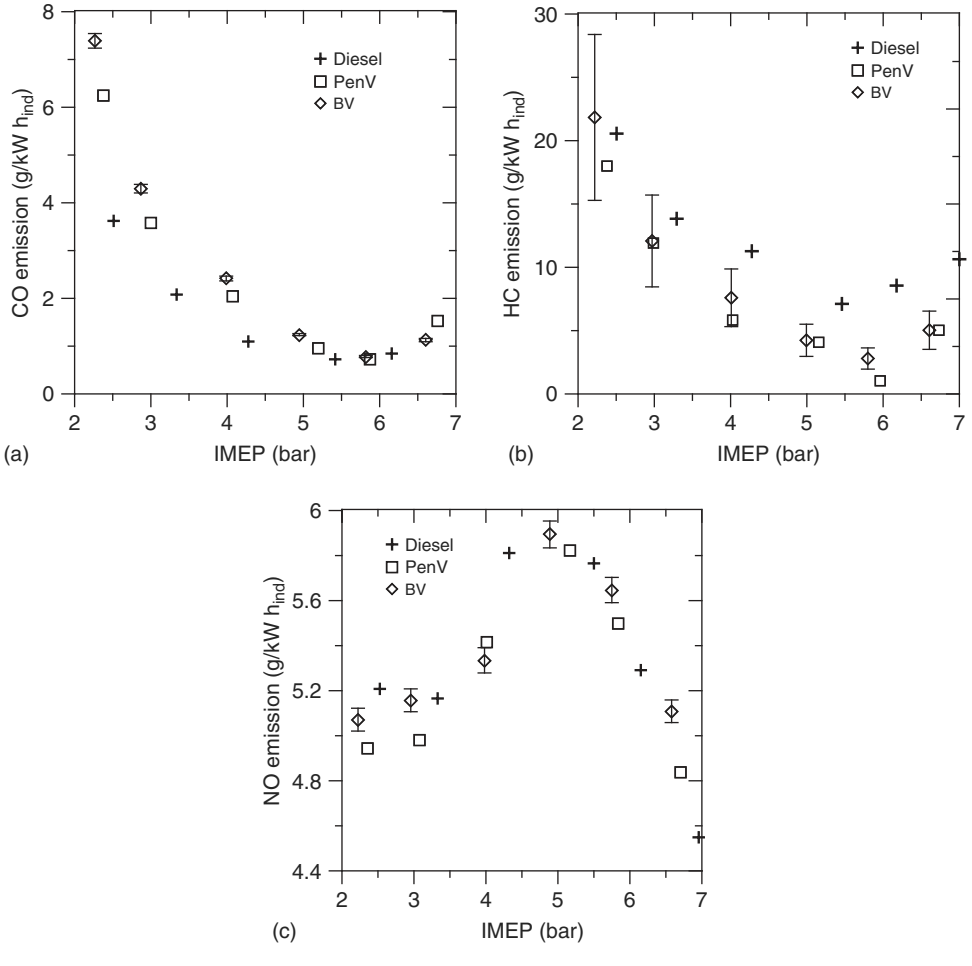

Figure 3.17 CO, unburnt HC, and NO emissions as a function of IMEP.

unburnt hydrocarbons (Figure 3.17b). However, in this case, the emissions of the blends are below those of pure diesel fuel even if they fall within the error bar. The NO emissions (Figure 3.17c) are similar for the blends and the pure diesel fuel. They increase with IMEP due to the increased thermal load and, around 5 bar, decrease. As NO emissions are generally considered as roughly proportional to the mass of fuel injected; this unexpected trend might be explained by the nonoptimal injection timing. The two properties of fuels that can increase the NO emissions are the cetane number, which slightly increases the pressure and temperature, and the oxygenated molecules, which have higher oxygen availability. Since there was no significant difference between the blends and pure diesel fuel, the small differences in these key factors compensate each other.

For the first time, the impact of using valerate blends for diesel combustion is evaluated in terms of particulate emissions by measuring soot FSN. Up to 5 bar, FSN values are very small for both the diesel fuel and the blends. But at a higher load, better combustion efficiency is achieved for the blends (see Figure 3.18). This behavior might be explained by the shorter ignition delay of diesel fuel for which the onset of combustion is in a slightly richer region, in particular when a larger amount of fuel is injected. The effect of valerates on the size distribution or composition of the particulate matter could not be assessed with this setup.

As a first evaluation of the potential of blending valerates in diesel fuel, these results show that there are no significant differences in terms of pollutant emissions and performances when adding 20 vol% of esters to diesel fuel, even if the cetane number and the autoignition are different. Although these experiments were performed without optimizing the process, as the injection timing was kept constant, the differences observed between the blends and the reference diesel

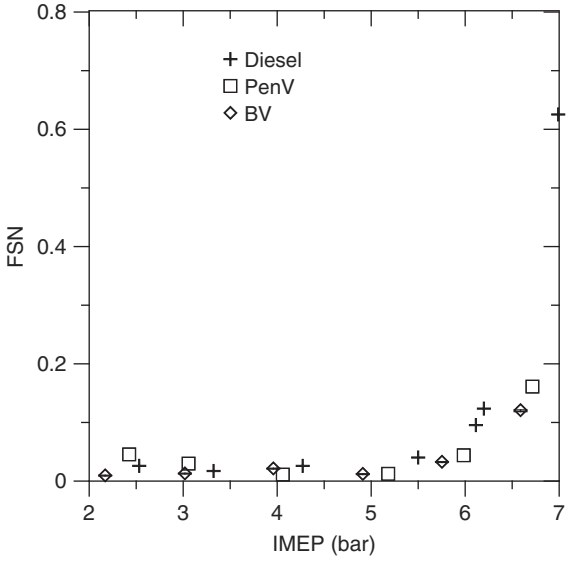

Figure 3.18 FSN values as a function of IMEP for both blends.

Table 3.3 Summary of the studies focused on the global performance of pure valerates and blend in IC engines.

Reference	Engine type	Operating conditions	Concentration in blend (or neat use)	Key conclusions	Mechanisms involved
Lange *et al.* [9]	SI engine (10 vehicles)	Road (500 km/day)	15% of EV in commercial gasoline	No difference in fuel consumption No effect on global behavior (fuel tank, emissions, etc.)	Global study
Contino *et al.* [17]	SI engine (0.4 l, single cylinder)	From 2 to 9 bar IMEP, 1200 rpm	20% MV and EV in PRF95	No visible effect for blended fuels (efficiency, CO_2, NO, CO, UHC)	Higher laminar burning speed
				For pure fuel higher CO_2	Higher research octane number and ignition delay
Mounaïm-Rousselle *et al.*, private communication (2014)	SI engine (0.5 l, single cylinder)	5 bar IMEP, 2000 rpm	100% EV	Higher consumption	Higher laminar burning speed
		3 bar IMEP, 1700 rpm	100% MV	Less UHC, CH_4, benzene emissions but higher ethylene and formaldehyde	Higher Research Octane Number and ignition delay oxygen contents
Contino *et al.* [17]	CI engine (0.4 l, single cylinder)	From 2 to 9 bar IMEP, 1500 and 2500 rpm	20% of BV and PenV in diesel	No visible effect for blended fuels (efficiency, CO, NO, CO, UHC, FSN)	Cetane number Higher ignition delay

fuel, in particular above 6 bar IMEP, are very small and would probably be further reduced by proper optimization.

All studies about the use of valerates as fuel are referenced in Table 3.3.

3.4 Production Pathways

As mentioned in Section 3.1, the generation of valerates from lignocellulose involves different processing steps. As underlined by Geboers *et al.* [2], the hydrolysis of cellulose remains a challenge. The method most commonly used

Table 3.4 Key performance indicators for the Lange *et al*. [28] three-step process.

Step	LA to GVL	GVL to VA	VA to valerate
Process	Hydrogenation	Hydrogenation	Esterification
Catalyst	Pt/TiO_2	Pt/ZSM-5	Acidic resin
Selectivity (%)	>95	>90	>95
Conversion (%)	>90	>50	>50
Residence time (h)	10	1	0.02

in the industry is hydrolysis by concentrated or diluted mineral acids, mainly sulfuric acid. Typically, 1% of sulfuric acid is used at elevated pressure (2.0 MPa) and temperature (493 K), with residence times of the order of several seconds. However, large-scale application of this method is complicated due to the recycling cost of the acid, reactor corrosion, and the formation of large amounts of neutralization waste. While new processes have emerged, such as solid acid catalytic systems for cellulose hydrolysis, drawbacks still remain due to the problem of adsorbed products and the rapid deactivation of the active sites of the catalysis.

Lange *et al.* [9] performed the conversion of LA to valerate in a flow reactor, using different catalysts to increase the conversion efficiency and the selectivity, as summarized in Table 3.4.

Assessing the global yield is therefore not straightforward, and each step can be improved by developing new processes, as recently underlined by Kon *et al.* [29].

For example, Lange *et al.* [9] also developed another process where LA is converted to EV in a single step. Cofeeding ethanol with LA as a physical or chemical mixture (in the form of ethyl levulinate) over a zeolite-based catalyst led to the coproduction of VA and EV in a single step. However, no conversion and selectivity ratios were indicated: a mixture of valerate and valeric acid was obtained. Moreover, some conditions such as temperature range, H_2 pressure range, and residence time need to be improved to develop an industrial green concept. Another test was the single-step conversion of GVL into PV ("diesel" valerate), which yielded 20–50% of selectivity.

Therefore, since Lange's paper in 2010, several researchers have been trying to develop new processes for one or several conversion steps in order to optimize conversion and selectivity.

Recently, Kon *et al.* [29] made a complete study of the effect of various catalyst parameters (such as the metal used) in the catalytic activity to convert LA into VA at 200 °C with 8 bar H_2 during 6 h. The best couple, which provided 100% of conversion, was Pt/HFMI. An interesting point is that the test was conducted not with 1 mmol but with 10 mmol. Conversion took 24 h, but as underlined by the authors, this could be due to the small amount of H_2. They also studied the synthesis of EV

and MV from LA and alcohols under an H_2 flow. After 3 h ethyl levulinate, one of the intermediates was totally consumed to produce EV. Only small quantities of VA and MTHF still remained. Therefore, complete conversion was achieved after 6 h with the catalyst Pt/HMFI at 200 °C and 8 bar H_2 with 78% of VA and 15% of GVL. Moreover, under solvent-free conditions, LA was converted to VA while in the presence of alcohols, the selectivity varied to form different valerates. The authors concluded that it could be a cost-effective method, thanks to the use of commercial materials such as Pt/HFMI.

A new kind of process, studied by Dong *et al.* [30], is based on the use of Brønsted acidic amino-acid ionic liquids to convert valeric acid into valerate. The idea is that these liquids allow a biphase esterification without any additional dehydrating agent. They tested many different configurations: three different liquid catalysts (proline bisulfate ($ProHSO_4$), glycine bisulfate, and alanine bisulfate), a temperature range from 25 to 80 °C, concentration of liquid catalyst ranging from 2% to 50% (based on mol of VA), and the VA/ethanol ratio. The highest conversion of VA to EV, more than 99.9%, was achieved with 50% of $ProHSO_4$, at a temperature of 80 °C, with an equal molar quantity of VA/ethanol mixture. The reaction was carried out for 7 h, and with this VA/ethanol ratio (1 : 1), due to the obtention of two-phase mixture, it is possible to select the VA easily. Therefore, $ProHSO_4$ can easily be isolated from the EV. After five cycles, the catalyst liquid appeared to maintain its ability to esterify VA. The authors also determined the properties of EV obtained and compared them with other fuels. The results are very promising: the energy density is higher than those of methanol, ethanol, GVL, and valeric acid. This confirms that EV is a promising biofuel candidate. This new process seems to be highly attractive and needs to be evaluated to produce other valerates.

A recent study conducted by Chan-Thaw *et al.* [31] is based on the use of a nonnoble metal, namely Cu, as an alternative catalyst and non Pt–zeolite one. The authors are the first to develop a one pot–one step process to obtain valerates (EV or PV) from conversion GVL to EV without the intermediate step of VA production. Different catalysts with the same Cu loading (8%) but different supports (SiZr, SiAl, and ZSM) were tested at 250 °C, with 10 bar of H_2. The highest conversion rate of 77% was obtained with Cu/SiZr after a 20 h run and yielded a mixture of 37% EV + 56% PV. Tests were also conducted with pentanol to increase the quantity of PV, and the conversion ratio reached 93% with more than 80% of PV. This could be a new way to generate biofuels from lignocellulose.

The valeric biofuels introduced by Lange *et al.* [28] are relatively new in the biofuel world. Very few studies have focused on the origin of the biomass; this is to say that the plant or the feedstock can be optimized for valerate production. Most of the processes focus on the production of LA and then GVL. For instance, Lange *et al.* [9] achieved a conversion efficiency of less than 5% for the conversion of the plant by hydrolysis to LA by using H_2SO_4 as catalyst. Rackemann and Doherty [32] did an interesting review of all the processes developed to provide

LA from lignocellulose. They pointed out that the production of LA from lignocellulose using mineral acids or metal catalysts suffers from several limitations: low yield, poor selectivity, the need for high temperature to convert the feedstocks, and high operating costs. They concluded that the "development of production methods has progressed from batch processes able to achieve <50% of the theoretical yield of levulinic acid to continuous processes incorporating recycling and utilizing multi-stages to optimize processing conditions to improve the yields to ~80% of the theoretical limit."

Recently, an interesting study was conducted by researchers from Pisa [33]. Using a high-yield catalytic route, they developed a process to produce LA and GVL directly from a plant. As giant reed is considered to be one of the suitable biomass sources for energy production, they improved their process on it by using a bifunctional (acid and hydrogenating) ruthenium-based catalytic system. Only 5 bar for H_2 and a temperature of 70 °C were required to perform hydrogenation. Initial results were very promising: almost 80% of GVL in mol (or 16.6% in weight) was produced, and the authors concluded that this indicates the great potential of GVL for biofuel production.

All the cited studies on the different processes to produce valerates are summarized in Table 3.5.

3.5 Outlook

Due to the properties of valerates, modern cars should be able to use valerates as additives in gasoline or diesel blends without any modification to their engines; moreover, the existing network of fueling stations could be used for their distribution. To use valerates as future fuels, however, further experiments are required to evaluate their real potential. Moreover, converting lignocellulose on a sufficiently large scale to be economically attractive and with significantly reduced CO_2 emissions is still challenging. The only company to consider the production of valerates from GVL by developing the new process so far is Shell (http://www.greencarcongress.com/2010/05/valerates-20100511.html). During the FP7 project DIBANET (Development of Integrated Biomass Approaches NETwork, 2008–2012), the United Kingdom, Brazil, and Chile were involved in developing novel sustainable technologies for the production and use of levulinic acid to make diesel-miscible fuels (via the esterification of ethanol with levulinic acid over solid acid catalysts), but not the production of valerates. The available level of technology is not high: as several steps of the processes are still at the optimization stage, the economic viability of the fuel production process has not yet been assessed.

Biofuel can be used as an additive to replace ethanol, for example, without any problem, but it is still not possible to determine whether it is less expensive and better for the world biomass than ethanol production. Moreover, it is still necessary to decide which plant, such as giant reed, would be the most appropriate to produce valerates.

Table 3.5 Different processes to obtain valeric esters.

Reference	Reactor type	Operating conditions	Concentration in solvent (or neat use)	Catalyst (if present)	Main reaction	Maximum yield and associated operating conditions/ catalyst
Lange *et al.* [9] GVL to EV	Flow reactor	Temperature 275–300 °C Pressure 10 bar Residence time	Ethanol	Pt or Pd/TiO_2	Hydrogenation + esterification	20–50% selectivity
Luo *et al.* [34] LA to EV		Temperature 200 °C Pressure 40 bar H_2 Residence time	Dioxane	Ru/TiO_2		VA + valerate 45.8% conversion
Pan *et al.* [35] LA to EV		Temperature 240 °C Pressure 40 bar H_2 Residence time	Ethanol	$Ru/SBA-SO_3H$	Hydrogenation	VA + EV 94% conversion
Kon *et al.* [29] LA to VA or EV		Temperature 200 °C Pressure 8 bar H_2 Residence time		Pt/HFMI		
Dong *et al.* [30] VA to EV	25 ml round bottomed flask	Temperature 80 °C Pressure Residence time 7 h	Ethanol	$ProHSO_4$	Esterification	99% conversion 100% selectivity (two phases)

3.6 Conclusions

Since Lange *et al.* announced their new process in 2010 to produce levulinic acid derivatives from lignocellulose, valerates have been studied in order to assess their capacity as potential fuels for car engines. These fuels are more suitable than GVL because they can provide biofuels of similar properties and that can be either blended with gasoline or diesel or used as fuels themselves. Recent works have focused on determining properties such as ignition delay, laminar burning speeds, and kinetic schemes to ensure their suitability as fuels. Few studies show that blends of valerates can be used as fuels in SI or compression engines without any drawback, but more real road experiments are needed to improve the real ability of valerates to be used as substitute fuels. As propyl valerate has properties between gasoline and diesel types, studies are also needed to improve it as a potential fuel.

Acknowledgments

The research leading to the authors has received funding from the European Research Council under the European Community's Seventh Framework Programme (FP7/2007–2013)/ERC grant agreement no. 291049 – 2G-CSafe.

Abbreviations

LA	levulinic acid
GVL	γ-valerolactone
VA	valeric acid
EV	ethyl valerate
MV	methyl valerate
PRV	propyl valerate
BV	butyl valerate
PV	pentyl valerate
BRON	blending research octane number
FAME	fatty acid methyl esters
MTHF	methyl tetrahydrofuran
EL	ethyl levulinate
MW	mass weight
LHV	latent heat vapor
AFR	air/fuel ratio
DCN	derived cetane number
CAD	crank angle degrees
CAX	CAD when X% of fresh gas are burnt
EPE	ethyl pentanoate
NTC	negative temperature coefficient
JSR	jet-stirred reactor
SI	spark-ignition engine
CI	compression-ignition engine
PRF	primary reference fuel (mixture of *iso*-octane and *n*-heptane)
PRF X	primary reference fuel mixture corresponding to RON index of X
HRR	heat release rate
SI	injection timing
IMEP	indicated mean effective pressure
TDC	top dead center

References

1. Azadi, P., Carrasquillo-Flores, R., Pagán-Torres, Y.J., Gürbüz, E.I., Farnood, R., and Dumesic, J.A. (2012) Catalytic conversion of biomass using solvents derived from lignin. *Green Chem.*, **14**, 1573.
2. Geboers, J.A., Van de Vyver, S., Ooms, R., Op de Beeck, B., Jacobs, P.A., and

Sels, B.F. (2011) Chemocatalytic conversion of cellulose: opportunities, advances and pitfalls. *Catal. Sci. Technol.*, **1**, 714–726.
3. Chalid, M. (2012) Levulinic acid as a renewable source for novel polymers. PhD thesis. Rijks Universiteit.
4. Leonard, R.H. (1956) Levulinic acid as a basic chemical raw material. *Ind. Eng. Chem.*, **48**, 1330–1341.
5. Mehdi, H., Fábos, V., Tuba, R., Bodor, A., Mika, L., and Horváth, I. (2008) Integration of homogeneous and heterogeneous catalytic processes for a multi-step conversion of biomass: from sucrose to levulinic acid, γ-valerolactone, 1,4-pentanediol, 2-methyl-tetrahydrofuran, and alkanes. *Top. Catal.*, **48**, 49–54.
6. Saiyasombat, W., Molloy, R., Nicholson, T.M., Johnson, A.F., Ward, I.M., and Poshyachinda, S. (1998) Ring strain and polymerizability of cyclic esters. *Polymer*, **39** (23), 5581–5585.
7. Serrano-Ruiz, J.C., Braden, D.J., West, R.M., and Dumesic, J.A. (2010) Direct conversion of cellulose to levulinic acid and gamma-valerolactone using solid acid catalysts. *Appl. Catal., B: Environ.*, **100**, 184–189.
8. Bond, J., Alonso, D.M., Wang, D., West, R.M., and Dumesic, J.A. (2010) Integrated catalytic conversion of γ-valerolactone to liquid alkenes for transportation fuels. *Science*, **327**, 1110–1114.
9. Lange, J.-P., Price, R., Ayoub, P.M., Louis, J., Petrus, L., and Clarke, L. (2010) Valeric biofuels: a platform of cellulosic transportation fuels. *Angew. Chem. Int. Ed.*, **49**, 4479–4483.
10. Masurier, J.B., Foucher, F., Dayma, G., and Dagaut, P. (2013) Homogeneous charge compression ignition combustion of primary reference fuels influenced by ozone addition. *Energy Fuels*, **27**, 5495–5505.
11. Dubreuil, A., Foucher, F., and Mounaim-Rousselle, C. (2009) Analysis of flame and OH natural emissions of *n*-heptane combustion in a homogeneous charge compression ignition HCCI engine effect of burnt gas dilution. *Energy Fuels*, **23** (3), 1406–1411.
12. Dayma, D., Gaïl, S., and Dagaut, P. (2008) Experimental and kinetic modeling study of the oxidation of methyl hexanoate. *Energy Fuels*, **22**, 1469–1479.
13. Dayma, G., Togbé, C., and Dagaut, P. (2009) Detailed kinetic mechanism for the oxidation of vegetable oil methyl esters: new evidence from methyl heptanoate. *Energy Fuels*, **23**, 4254–4268.
14. Hadj-Ali, K., Crochet, M., Vanhove, G., Ribaucour, M., and Minetti, R. (2009) A study of the low temperature autoignition of methyl esters. *Proc. Combust. Inst.*, **32**, 239–246.
15. El-Nahas, A.M., Navarro, M.V., Simmie, J.M., Bozzelli, J.W., Curran, J.W., Dooley, S., and Metcalfe, S. (2007) Enthalpies of formation, bond dissociation energies and reaction paths for the decomposition of model biofuels: ethyl propanoate and methyl butanoate. *J. Phys. Chem. A*, **111**, 3727–3739.
16. Hayes, C.J. and Burgess, D.R. Jr., (2009) Exploring the oxidative decompositions of methyl esters: methyl butanoate and methyl pentanoate as model compounds for biodiesel. *Proc. Combust. Inst.*, **32**, 263–270.
17. Contino, F., Dayma, G., Dagaut, P., Halter, F., Foucher, F., and Mounaïm-Rousselle, C. (2013) Engine Performances and Emissions of Second-Generation Biofuels in Spark Ignition Engines: The Case of Methyl and Ethyl Valerates. SAE Technical Paper, issue 2013-24-0098.
18. Shmakov, A.G., Gerasimov, I.E., Knyazkov, D.A., Bolshova, T.A., Shvartsberg, V.M., Korobeinichev, O.P., Hansen, N., and Westbrook, C.K. (2014) Experimental and modeling study of premixed methyl pentanoate flames stabilized at atmospheric and low-pressure conditions. 8th International Seminar on Flame Structure, Berlin, September 21–24, 2014.
19. Knyazkov, D.A., Gerasimov, I.E., Korobeinichev, O.P., Shmakov, A.G., and Hansen, N. (2014) Structure of a low

pressure ethyl pentanoate (ethyl valerate) flame studied by flame sampling molecular beam mass spectrometry with VUV photoionization and numerical simulation. 8th International Seminar on Flame Structure, Berlin, September 21–24, 2014.
20. Mbuyi Katshiatshia, H., Dias, V., and Jeanmart, H. (2014) Experimental study of rich ethyl valerate flame at low temperature. 8th International Seminar on Flame Structure, Berlin, September 21–24, 2014.
21. Dayma, G., Halter, F., Foucher, F., Togbé, C., Mounaim-Rousselle, C., and Dagaut, P. (2012) Experimental and detailed kinetic modeling study of ethyl pentanoate (ethyl valerate) oxidation in a jet stirred reactor and laminar burning velocities in a spherical combustion chamber. *Energy Fuels*, **26**, 4735–4748.
22. Contino, F., Foucher, F., Mounaïm-Rousselle, C., and Jeanmart, H. (2011) Combustion characteristics of tri- component fuel blends of ethyl acetate, ethyl propionate, and ethyl butyrate in homogeneous charge compression ignition (HCCI). *Energy Fuels*, **25** (4), 1497–1503.
23. Contino, F., Jeanmart, H., Lucchini, T., and D'Errico, G. (2011) Coupling of in situ adaptive tabulation and dynamic adaptive chemistry: an effective method for solving combustion in engine simulations. *Proc. Combust. Inst.*, **33** (2), 3057–3064.
24. Contino, F., Dagaut, P., Dayma, G., Halter, F., Foucher, F., and Mounaïm-Rousselle, C. (2013) Combustion and emissions characteristics of valeric biofuels in a compression ignition engine. *J. Energy Eng.*, **140** (3), A4014013.
25. Curran, H.J., Gaffuri, P., Pitz, W.J., and Westbrook, C.K. (2002) A comprehensive modeling study of iso-octane oxidation. *Combust. Flame*, **129** (3), 253–280.
26. Contino, F., Masurier, J.B., Foucher, F., Lucchini, T., D'Errico, G., and Dagaut, P. (2014) CFD simulations using the TDAC method to model iso-octane combustion for a large range of ozone seeding and temperature conditions in a single cylinder HCCI engine. *Fuel*, **137** (1), 179–184.
27. Broustail, G., Seers, P., Halter, F., Moréac, G., and Mounaïm-Rousselle, C. (2011) Experimental determination of laminar burning velocity for butanol and ethanol iso-octane blends. *Fuel*, **90**, 1–6.
28. Lange, J.P., Vestering, J.Z., and Haan, R.J. (2007) Towards 'bio-based' nylon: conversion of gamma-valerolactone to methyl pentenoate under catalytic distillation conditions. *Chem. Commun.*, (33), 3488–3490.
29. Kon, K., Onodera, W., and Shimizu, K.I. (2014) Selective hydrogenation of levulinic acid to valeric acid and valeric biofuels by a Pt/HMFI catalyst. *Catal. Sci. Technol.*, **4**, 3227–3234. doi: 10.1039/C4CY00504J, Advance Article.
30. Dong, L.-L., He, L., Tao, G.-H., and Hu, C. (2013) High yield of ethyl valerate from the esterification of renewable valeric acid catalyzed by amino acid ionic liquids. *RSC Adv.*, **3**, 4806–4813.
31. Chan-Thaw, C.E., Marelli, M., Psaro, R., Ravasio, N., and Zaccheria, F. (2013) New generation biofuels: γ-valerolactone into valeric esters in one pot. *RSC Adv.*, **3**, 1302–1306.
32. Rackemann, D.W. and Doherty, W.O.S. (2011) The conversion of lignocellulosics to levulinic acid. *Biofuels, Bioprod. Biorefin.*, **5** (2), 115–126.
33. Raspolli Galletti, A.M., Antonetti, C., Ribechini, E., Colombini, M.P., Nassi o Di Nasso, N., and Bonari, E. (2013) From giant reed to levulinic acid and gamma-valerolactone: a high yield catalytic route to valeric biofuels. *Appl. Energy*, **102**, 157–162.
34. Luo, W.H., Deka, U., Beale, A.M., Van Eck, E.R.H., and Werchuyssen, P.C.A. (2013) Ruthenium-catalyzed hydrogenation of levulinic acid: Influence of the support and solvent on catalyst selectivity and stability. *J. Catal.*, **301**, 175–186.
35. Pan, T., Deng, J., Xu, Q., Xu, Y., Guo, Q.-X., and Fu, Y. (2013) Catalytic conversion of biomass-derived levulinic acid to

valerate esters as oxygenated fuels using supported ruthenium catalysts. *Green Chem.*, **15**, 2967–2974.

36. Bozell, J.J. and Petersen, G.R. (2010) Technology development for the production of biobased products from biorefinery carbohydrates; the US Department of Energy's "Top 10 revisited". *Green Chem.*, **12**, 539–554.